

Generate, Segment and Replace: Towards Generic Manipulation Segmentation

Peng Zhou¹ Bor-Chun Chen¹ Xintong Han² Mahyar Najibi¹ Larry S. Davis¹
¹University of Maryland, College Park ²Malong Technologies

{pengzhou, sirius}@umd.edu xintong.han@malong.com najibi@cs.umd.edu lsd@umiacs.umd.edu

Abstract

It has been witnessed an emerging demand for image manipulation segmentation to distinguish between fake images produced by advanced photo editing software and authentic ones. In this paper, we describe an approach based on semantic segmentation for detecting image manipulation. The approach consists of three stages. A generation stage generates hard manipulated images from authentic images using a Generative Adversarial Network (GAN) based model by cutting a region out of a training sample, pasting it into an authentic image and then passing the image through a GAN to generate harder true positive tampered region. A segmentation stage and a replacement stage, sharing weights with each other, then collaboratively construct dense predictions of tampered regions. We achieve state-of-the-art performance on four public image manipulation detection benchmarks while maintaining robustness to various attacks.

1. Introduction

Manipulated photos are ubiquitous on social media due to the development of editing tools and generative adversarial models [14, 35]. People harness these images for various purposes, even including images for fake news. Thus, there is an increasing demand for automatic image manipulation detection. In this paper, we treat the problem of image manipulation detection as a semantic segmentation problem, using GANs [10] to augment scarce training data for this task.

In contrast to the standard semantic image segmentation, manipulation segmentation depends more on artifacts at boundaries than on semantic contents [2, 38]. One challenge to directly adopting semantic image segmentation networks to this task is that the space of manipulations is very diverse. For instance, manipulation techniques include *copy-move* which copies and pastes image regions within the same image (the second column in Figure 1), and *splicing* which copies a region from one image and pastes it to another image (the rest columns in Figure 1). Addition-

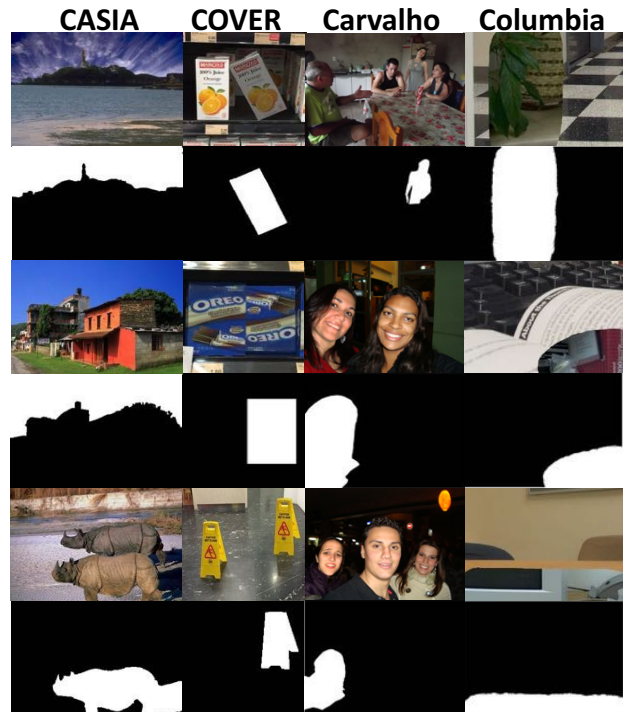


Figure 1. Examples of manipulated images across different datasets. Columns from left to right are images in CASIA [8], COVER [34], Carvalho [5], and Columbia [21]. The odd rows are manipulated images and the even rows are the ground truth masks. Different datasets contain different distributions (from animals, person to non-object regions), manipulation techniques (from copy-move (the second column) to splicing (the rest columns)) and post-processing methods (from no post-processing to various processes including filtering, illumination, and blurring).

ally, a variety of post-processing techniques such as compression, blurring and various color transformations can be employed to visually camouflage the obvious artifacts of a manipulation. See Figure 1 for visualization examples. Finally, existing datasets [21, 7, 8, 34, 5] have very small training data due to the time needed by humans to carefully generate manipulated images.

Most existing tamper detection methods [12, 38, 22, 26] utilize discriminative features like image metadata, noise

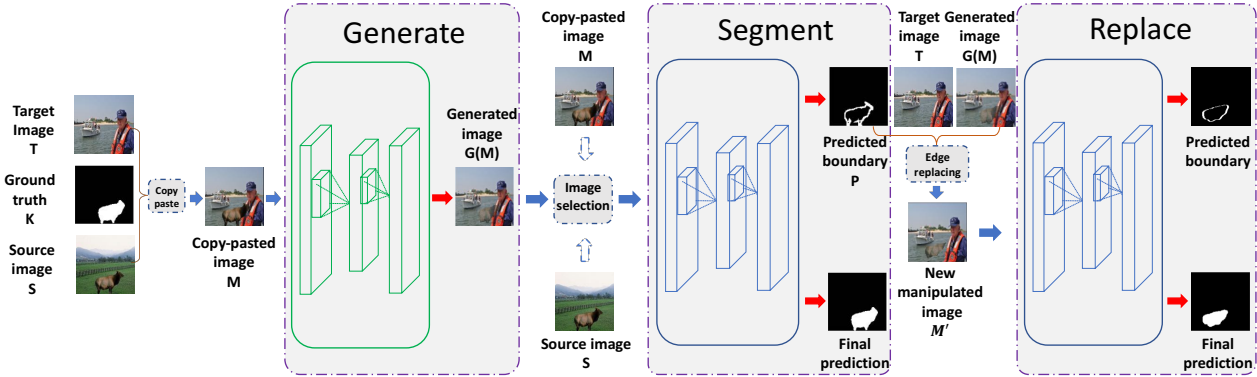


Figure 2. GSR-Net framework overview. Given a source image S , an authentic target image T , and the ground truth mask K , the generation stage generates hard example $G(M)$ starting from a simple copy-pasting image M . Selecting from training images, copy-pasted images and generated images as input, the segmentation stage learns to segment the boundary artifacts and fill the interior to produce the final prediction. The replacement stage creates a novel tampered image with new boundary artifacts by replacing the predicted manipulated boundaries of segmentation stage with original authentic regions and learns to make a new prediction. The replacement stage shares weights with the segmentation stage.

models, or color artifacts due to, for example, Color Filter Array (CFA) inconsistencies, to localize the artifacts of manipulation. However, the generalization of these networks is limited when extended to a large variety of manipulations. To address this challenge, we employ a GAN to create manipulated images using widely available authentic images and avoid overfitting on semantic contents through creating and spotting new boundary artifacts sequentially.

To this end, we propose an end-to-end manipulation segmentation network called GSR-Net which has three components – a generation stage, a segmentation stage and a replacement stage. The architecture of GSR-Net is shown in Figure 2. The generation stage produces both easy and hard manipulation examples to simulate post-processing applied to the manipulated images. Benefitting from numerous authentic background candidates, the generation stage also provides a diverse data distribution to avoid over-fitting on limited training data. Taking as input the generated, copy-pasted or manipulated images, the segmentation stage localizes manipulated regions by learning to focus on boundary artifacts. Eventually, the network segments the manipulated regions by learning to fill the interior of the boundaries. To further prevent the network from focusing on semantic contents, the replacement stage replaces the predicted manipulated boundaries with authentic background and pushes the new manipulated images through the segmentation network. Consequently, the segmentation network predicts the new manipulated boundaries and interior regions to further focus its attention on boundary artifacts as the clues to manipulation. We train the entire network jointly in an end-to-end fashion. Finally, learning with a large variety of manipulation artifacts provided by both the generation and replacement stage, GSR-Net experimentally exhibits very good generalization ability.

We evaluate GSR-Net on four public benchmarks and show that it outperforms state-of-the-art methods. Experiments with two different post-processing attacks further demonstrate the robustness of GSR-Net.

In summary, the contributions of this paper are 1) Utilizing a generative model with authentic images to create manipulated images to boost the generalization ability of a semantic segmentation network for manipulation detection. 2) Proposing a manipulation specific replacement strategy to focus the network on manipulation artifacts. 3) Extensive experiments which show the proposed method achieves state-of-the-art performance on four different public benchmarks while maintaining robustness to various attacks.

2. Related Work

Image Manipulation Segmentation. Park *et al.* [22] train a network to find JPEG compression discrepancies between manipulated and authentic regions. Zhou *et al.* [37, 38] harness noise features to find inconsistencies within a manipulated image. Huh and Liu *et al.* [12] treat the problem as anomaly segmentation and use metadata to locate abnormal patches. The features used in these works are based on the assumption that manipulated regions are from a different image, which is not the case in copy-move manipulation. However, our method directly focuses on general artifacts in the RGB channel without specific feature extraction and thus can be applied to copy-move segmentation. More related, Salloum *et al.* [26] and Bappy *et al.* [2] show the potential of boundary artifacts in different image manipulation techniques. Salloum *et al.* [26] adopt a Multi-task Fully Convolutional Network (MFCN) [19] to manipulation segmentation by providing both segmentation and edge annotations. Bappy *et al.* [2] design a Long Short-

Term Memory (LSTM) [11] based network to identify RGB boundary artifacts at both the patch and pixel level. These methods motivate our method to exploit boundary artifacts as the main cues in manipulation segmentation. However, since the limited available data reduces the generalization of the pixel-level approaches, we propose an effective method to generate manipulated images from authentic ones.

GAN Based Image Editing. GAN based image editing approaches have witnessed a rapid emergence and impressive results recently [30, 16, 23, 31]. Prior and concurrent works force the output of GAN to be conditioned on input images through extra regression losses (e.g., ℓ_2 loss) or discrete labels. In particular, Tsai *et al.* [30] generate natural composite images using both scene parsing and harmonized ground truth. Pathak *et al.* [23] present a context encoder trained with reconstruction plus an adversarial loss to inpaint missing image contents. In contrast to these methods, we generate manipulated images for better generalization ability of a manipulation segmentation network.

Adversarial Training. Discriminative feature learning has motivated recent research on adversarial training on several tasks. Shrivastava *et al.* [27] propose a simulated and unsupervised learning approach which utilizes synthetic images to generate realistic images. Wang *et al.* [32] boost the performance on occluded and deformed objects through an online hard negative generation network. Wei *et al.* [33] investigate an adversarial erasing approach to learn dense and complete semantic segmentation. Le *et al.* [17] propose an adversarial shadow attenuation network to make correct predictions on hard shadow examples. Inspired by these works and taking into account the demand for diverse examples in the image manipulation segmentation task, we generate both hard and easy examples to help the network learn manipulation artifacts.

3. Approach

Generation, segmentation, and replacement are the three principal components in our approach. As illustrated in Figure 2, the generation stage generates manipulated images with subtle artifacts starting from copying and pasting a manipulated region to an authentic image. Taking as input these generated images, the segmentation stage localizes the manipulated regions based on clues around their boundaries, and fills their interiors. Original manipulated images in the training data and the copy-pasted images are utilized to provide a large variety of manipulations. To suppress semantic contents and enhance attention on boundary artifacts, we utilize a replacement stage that replaces the predicted manipulated boundaries by the original authentic image regions and subsequently feeds back the new manipulated image to the segmentation stage as a new training sample. In the following, we describe these components in detail.

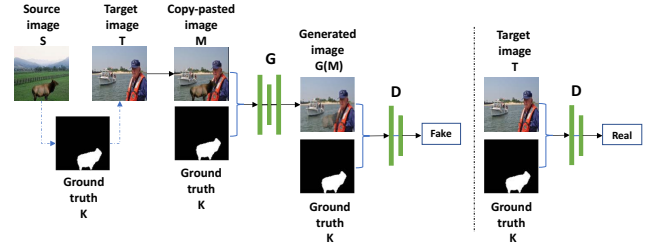


Figure 3. Generation stage. The generator G learns to refine the manipulated regions to match with authentic regions given a copy-pasted image M and the position mask where to refine. M is created using the source image S , ground truth mask K and authentic target image T . The discriminator D learns to classify manipulated images from authentic ones.

3.1. Generation

The generation stage is a GAN mimicking the process of image manipulation. (See Figure 3)

3.1.1 Generator

The structure of the generator is based on U-Net [25] which is given as input both copy-pasted images and ground truth masks. To prepare the input images, we start with the training samples in manipulation datasets (CASIA 2.0 in our case). Given a training image S in the dataset, the ground truth binary mask K for S and an authentic target image T from a clean dataset (COCO dataset [18] in this paper), we first create a copy-pasted image M by taking S as foreground and T as background:

$$M = K \odot S + (1 - K) \odot T, \quad (1)$$

where \odot represents pointwise multiplication.

Inspired by Poisson blending [24], we optimize the generator to blend the copy-pasted regions with respect to an objective which matches the final manipulated regions with the target image while satisfying a boundary constraint. This allows us to jointly train the entire network efficiently in an end-to-end fashion. Formally, the final value of pixel i in the manipulated regions is

$$m_i = \arg \min_{m_i} \sum_{s_i \in S, \mathcal{N}_i \subset S} \|\nabla m_i - \nabla s_i\|_2 + \sum_{s_i \in S, \mathcal{N}_i \not\subset S} \|m_i - t_i\|_2, \quad (2)$$

where ∇ denotes the gradient, \mathcal{N}_i is the neighborhood (e.g., up, down, left and right) of the pixel at position i , m_i is the pixel in M , s_i is the pixel in S and t_i is the pixel in T . To maintain background regions, we utilize ℓ_1 loss as in [14]

to reconstruct the background:

$$L_{bg} = \frac{1}{N_{bg}} \sum_{t_i \in T, k_i=0} \|m_i - t_i\|_1, \quad (3)$$

where N_{bg} is the total number of pixels in the background, and k_i is the value in mask K at position i . To maintain the shape of manipulated regions, we apply a Laplacian operator to the pasted regions and reconstruct the gradient of this region to match the source region:

$$L_{grad} = \frac{1}{N_{fg}} \sum_{s_i \in S, k_i=1} \|\Delta m_i - \Delta s_i\|_1, \quad (4)$$

where Δ denotes the Laplacian operator and N_{fg} is the total number of pixels in pasted regions. To further constrain the shape of pasted regions, we add an additional edge loss as denoted by

$$L_{edge} = \frac{1}{N_{edge}} \sum_{s_i \in S, e_i=1} \|m_i - s_i\|_1, \quad (5)$$

where N_{edge} is the total number of boundary pixels and e_i is the value of the edge mask at position i , which is obtained by the absolute difference between a dilation and an erosion on K . To generate realistic manipulated images, we add an adversarial loss L_{adv} as explained in section 3.1.2 on the generator to introduce variations on the value of the pasted regions through fooling the discriminator.

The loss function of the generator is summarized as

$$L_G = L_{bg} + \lambda_{grad} L_{grad} + \lambda_{edge} L_{edge} + \lambda_{adv} L_{adv}, \quad (6)$$

where λ_{grad} , λ_{edge} , and λ_{adv} are parameters which control the importance of the corresponding loss terms. Conditioned on this constraint, the generator preserves background and texture information of pasted regions while blending the manipulated regions with the background.

3.1.2 Discriminator

The structure of the discriminator is based on the PatchGAN discriminator [14] with the assumption that the manipulated regions are smaller than the background and require more local information for classification. More specifically, the discriminator makes a decision on an $N \times N$ patch scale as it has a fully convolutional layer at the last layer. The discriminator distinguishes the authentic image T as real and the generated image $G(K, M)$ as fake by maximizing:

$$L_{adv} = \mathbb{E}_T \log(D(K, T)) + \mathbb{E}_M [1 - \log(D(K, G(K, M)))], \quad (7)$$

where K is concatenated with M or T as the input to the discriminator.

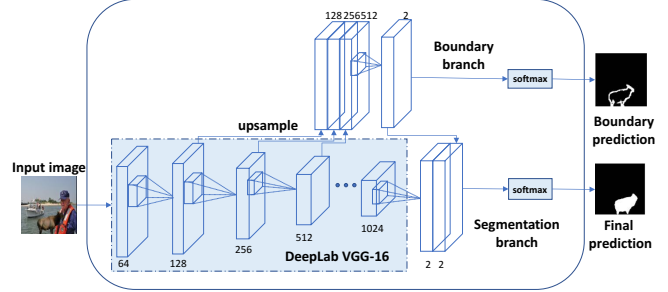


Figure 4. Segmentation stage. We concatenate lower level features to predict boundary artifacts and then concatenate back the boundary feature to the segmentation branch to learn to fill the interior of boundaries. The backbone is DeepLab VGG-16.

3.2. Segmentation

Our approach depends on no specific segmentation network and can be applied to any off-the-shelf model structure for manipulation segmentation. For simplicity, we adopt the public available VGG-16 [28] based DeepLab model [3] to the manipulation segmentation task. The network structure is depicted in Figure 4, consisting of a boundary branch predicting the manipulated boundaries and a segmentation branch predicting the interior. In particular, to enhance attention on boundary artifacts, we introduce boundary information by subtracting the erosion from the dilation of the binary ground truth mask to obtain the boundary mask. We then predict this boundary mask through concatenating bi-linearly up-sampled intermediate features and passes them to a 1×1 convolutional layer to form the boundary branch. We finally concatenate back the output features of the boundary branch with the up-sampled features of the segmentation branch. With the boundary information, the segmentation branch learns to fill the interior. Empirically, we noticed such a multi-task learning helps the generalization of the final model. Only the segmentation branch output is used for evaluation during inference. We select the easy examples M , generated examples $G(M)$ and training samples S in the dataset as input to the segmentation network to provide large variations of manipulations. The loss function of the segmentation network is an average, two class softmax cross entropy loss.

3.3. Replacement

The replacement stage can be viewed as an augmented segmentation stage, where new boundary artifacts are generated and then detected. Taking into account the fact that boundary artifacts are more important than semantic contents in manipulation segmentation, the replacement stage utilizes the prediction of the segmentation stage to produce new boundary artifacts without additional annotations during training. As illustrated in Figure 2, given a target image T in which the manipulated regions was inserted, the

manipulated image M (could also be the generated image $G(M)$) and the manipulated boundary prediction P by the segmentation stage, we replace the pixels in predicted boundaries by the authentic regions in T and create a novel manipulated image:

$$M' = T \odot P + M \odot (1 - P), \quad (8)$$

where M' is the novel manipulated image with new boundary artifacts. The corresponding segmentation ground truth now becomes

$$K' = K - K \odot P, \quad (9)$$

where K' is the new manipulated mask for M' . The new boundary artifact mask can be extracted in the same way as the previous step. Taking as input the new manipulated images, the same segmentation network as in Figure 4 then learns to predict the new manipulated boundaries and interior regions. Similar to prior work on adversarial mining [33], the replacement stage also allows multiple replacing operations with a tradeoff between training time and performance. However, the difference is that the segmentation network in the replacement stage shares weights with that in the segmentation stage. The weight sharing enables us to use a single segmentation network at the inference time while benefitting from the replacement stage during training. As a result, the network pays more attention on boundary artifacts with no additional cost at inference time.

4. Experiments

We evaluate the performance of GSR-Net on four public benchmarks and compare it with the state-of-the-art methods. We also analyze its robustness under several attacks.

4.1. Implementation Details

GSR-Net is implemented in Tensorflow [1] and trained on an NVIDIA GeForce TITAN P6000. The input to the generation network (both generator and discriminator) is resized to 256×256 . We apply \tanh to the output of the generator and match the input range of the segmentation network. The discriminator has the same structure as 70×70 PatchGAN without the batch normalization layers. We add batch normalization [13] to the DeepLab VGG-16 model. The segmentation network is fine-tuned from ImageNet [6] pre-trained weights and the generation network is trained from scratch. We use Adam [15] optimizer with a fixed learning rate of 0.0001 for all the subnetworks. Optimizer of the generator, discriminator and segmentation network are updated in an alternating fashion. To avoid overfitting, weight decay with a factor of 5×10^{-5} and 50% dropout [29] are applied on the segmentation network. The hyperparameters of $(\lambda_{grad}, \lambda_{edge}, \lambda_{adv})$ are set to (1, 2, 5) empirically to balance the loss values. For simplicity, only random flipping augmentation is applied during training. We

feed the copy-pasted images, generated images as well as the training samples to the segmentation network. However, we only apply the replacement stage to samples from the training dataset (CASIA 2.0 in our case) based on the experience that adding the replacement operation on generated examples increases the instability of the generation network. We train the whole network jointly for 50K iterations with a batch size of 4.

Only the segmentation network is used for inference and we directly use the segmentation branch as the final prediction. Due to the small batch size used during training, we utilize instance normalization as in [14] on every test image. After prediction, instead of using mean-shift as in [12], we simply dilate and threshold connected components to remove small noisy particles.

4.2. Datasets and Experiment Setting

Datasets. We evaluate our performance on four datasets as below:

- **Columbia [21]:** Columbia is a splicing dataset with 180 uncompressed images taken by different cameras. No post-processing is added after splicing regions to other images. The manipulated regions are usually not objects and have arbitrary shapes.

- **COVER [34]:** COVER focuses on copy-move manipulation and has 100 images. The manipulation objects are used to cover similar objects in the original authentic images and thus are challenging for humans to recognize visually without close inspection.

- **CASIA [8, 7]:** CASIA has two versions. CASIA 1.0 contains 921 manipulated images including splicing and copy move. The objects are carefully selected to match with the context in the background. Cropped regions are subjected to post-processing including rotation, distortion, and scaling. CASIA 2.0 is a more complicated dataset with 5123 images. Manipulations include splicing and copy move. Post-processing like filtering and blurring is applied to make the regions visually realistic. The manipulated regions cover animals, textures, natural scenes, *etc.* We use CASIA 2.0 to train our network and test it on CASIA 1.0.

- **Carvalho [5]:** Carvalho is a manipulation dataset designed to conceal illumination differences between manipulated regions and authentic regions. The dataset contains 100 images and all the manipulated objects are people. Contrast and illumination are adjusted as post-processing.

Evaluation Metrics. We use pixel-level F1 score and MCC as the evaluation metrics when comparing to other approaches. For fair comparison, following the same measurement as [26, 12, 38], we vary the prediction threshold to get binary prediction mask and report the optimal score over the whole dataset.

Dataset	Carvalho [5]		Columbia [21]		COVER [34]		CASIA [7]	
Metrics	MCC	F1	MCC	F1	MCC	F1	MCC	F1
NOI [20]	0.255	0.343	0.412	0.574	0.172	0.269	0.180	0.263
CFA [9]	0.164	0.292	0.233	0.476	0.050	0.190	0.108	0.207
MFCN [26]	0.408	0.480	0.479	0.612	-	-	0.520	0.541
RGB-N [38]	0.261	0.383	0.594	0.705	0.334	0.379	0.364	0.408
EXIF-consistency [12]	0.420	0.520	0.800	0.872	0.102	0.276	0.127	0.204
DeepLab (baseline)	0.343	0.420	0.458	0.643	0.304	0.376	0.435	0.474
GSR-Net (ours)	0.462	0.525	0.733	0.829	0.439	0.489	0.553	0.574

Table 1. MCC and F_1 score comparison on four standard datasets. ‘-’ denotes that the result is not available in the literature.

4.3. Main Results

We fine-tune our model on CASIA 2.0 from the ImageNet pre-trained model and test the performance on the aforementioned four datasets. We compare with the methods described below:

- NoI** [20]: A noise inconsistency method which predicts regions as manipulated where the local noise is inconsistent with authentic regions. We use the code provided by Zampoglou *et al.* [36] for evaluation.

- CFA** [9]: A CFA based method which estimates the internal CFA pattern of the camera for every patch in the image and segments out the regions with anomalous CFA features as manipulated regions. The evaluation code is based on Zampoglou *et al.* [36].

- RGB-N** [38]: A two-stream Faster R-CNN based approach which combines features from the RGB and noise channel to make the final prediction. We train the model on CASIA 2.0 using the code provided by the authors¹.

- EXIF-consistency** [12]: A self-consistency approach which utilizes metadata to learn features useful for manipulation localization. The prediction is made patch by patch and post-processing like mean-shift [4] is used to obtain the pixel-level manipulation prediction. We use the code provided by the authors² for evaluation.

- MFCN** [26]: A multi-task FCN based method which harnesses both an edge mask and segmentation mask for manipulation segmentation. Hole filling is applied for the edge branch to make the prediction. The final decision is the intersection of the two branches. We directly report the results from the paper since the code is not publicly available.

- DeepLab**: Our baseline model which directly adopts DeepLab VGG-16 model to manipulation segmentation task. No generation, boundary branch or replacement stage is added.

- GSR-Net**: Our full model combining generation, segmentation and replacement for manipulation segmentation.

The comparison results in Table 1 highlight the advantage of GSR-Net. For supervised methods [38, 26], we train the model on CASIA 2.0 and evaluate on all the

four datasets. For others [20, 9, 12], we directly test the model on all datasets. GSR-Net outperforms other approaches by a large margin on COVER, suggesting the advantage of our network on copy-move manipulation. Also, GSR-Net has an improvement on CASIA 1.0 and Carvalho. Even though EXIF-consistency outperforms GSR-Net on Columbia, results in section 4.5 demonstrate our advantage with respect to robustness to compression and scaling over EXIF-consistency. Moreover, in terms of computation time, EXIF-consistency takes 160 times more computation (80 seconds for an 800×1200 image on average) than ours (0.5s per image). Compared to boundary artifact based methods, our GSR-Net outperforms MFCN by a large margin, indicating the effectiveness of the generation and replacement stages. In addition to that, no hole filling is required since our approach does not perform late fusion with the boundary branch, but utilizing boundary artifacts to guide the segmentation branch instead.

Our method outperforms the baseline model by a large margin, showing the effectiveness of the proposed generation, segmentation and replacement stages. More details are discussed in section 4.4.

4.4. Ablation Studies

We quantitatively analyze the influence of each component in GSR-Net in terms of F1 score.

- DL + cp**: DeepLab VGG-16 model with just the segmentation output, using simple copy-pasted (no generator) and CASIA 2.0 images during training.

- DL + g**: DeepLab VGG-16 model with just the segmentation output, using generated and CASIA 2.0 images during training.

- DL + G edge**: Generation and DeepLab VGG-16 network only predict boundary masks. Hole filling is applied to generate the final pixel level prediction.

- DL + G**: DeepLab VGG-16 model with just the segmentation output, using both copy-pasted, generated and CASIA 2.0 images during training.

- DL + GDA**: DeepLab VGG-16 model with only segmentation output, using both copy-pasted, generated and CASIA 2.0 images during training. We augment manipulated

¹<https://github.com/pengzhou1108/RGB-N>

²<https://github.com/minyoungg/selfconsistency>

Dataset	Carvalho	Columbia	COVER	CASIA
DeepLab	0.420	0.643	0.376	0.474
DL + cp	0.446	0.756	0.410	0.503
DL + g	0.460	0.686	0.434	0.506
DL + G edge	0.434	0.684	0.447	0.472
DL + G	0.472	0.789	0.444	0.507
DL + GDA	0.480	0.780	0.445	0.535
DL + GR	0.487	0.778	0.455	0.549
DL + GR2	0.500	0.799	0.440	0.562
GS-Net	0.515	0.800	0.455	0.545
GSR-Net	0.525	0.829	0.489	0.574

Table 2. Ablation studies on four datasets. Each entry is the F1 score tested on individual dataset.

Dataset	Carvalho	Columbia	COVER	CASIA
cp + S	0.343	0.684	0.351	0.242
cpg + S	0.354	0.726	0.381	0.270
cpg + SR	0.418	0.731	0.355	0.331
GSR-Net	0.525	0.829	0.489	0.574

Table 3. Manipulation segmentation comparison with COCO annotations. Each entry is the F1 score.

images from the beginning by replacing the boundary artifact regions with the regions in target images using ground truth masks.

- DL + GR**: DeepLab VGG-16 model with only segmentation output, using both copy-pasted, generated and CASIA 2.0 images during training. The replacement stage is added.
- DL + GR2**: Same as **DL + GR** except that the replacement stage is applied twice.
- GS-Net**: Generation and segmentation network with boundary artifact guided manipulation segmentation. No replacement stage is incorporated.

Table 2 displays the results. Starting from our baseline model, simply adding copy-pasted images (**DL + cp**) achieves improvement due to broadening the manipulation distribution. In addition, replacing copy-pasted images with generated images (**DL + g**) also shows improvement compared to **DL + cp** on most of the datasets as it refines the boundary from naive copy-pasting. However, the performance drops on Columbia because boundary artifacts are refined to be more realistic and the network tends to forget easy examples when training on hard ones. As expected, adding both copy-pasted images and generated hard examples (**DL + G**) is more useful because the network has access to a larger distribution of manipulation. Compared with direct augmentation in **DL + GDA**, the replacement stage (**DL + GR**) has the advantage of mining hard examples since it harnesses predicted manipulated boundaries. Applying the replacement stage one or two times (**DL + GR2**) shows effectiveness on several of the datasets. Our **GSR-Net** applies the replacement stage for only one iteration as a trade-off between training time and performance.

The results also indicate the impact of boundary guided

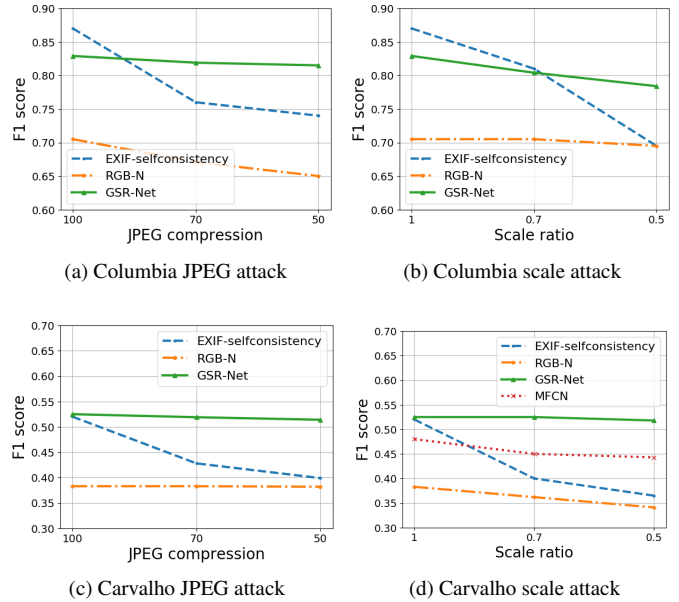


Figure 5. Analysis of robustness under different attacks. Attacks with JPEG compression consists of quality factors of 70 and 50; scale attacks use scaling ratios of 0.7 and 0.5. (a) JPEG compression attacks on Columbia. (b) Scale attacks on Columbia. (c) JPEG compression attacks on Carvalho. (d) Scale attacks on Carvalho.



Figure 6. Qualitative visualization of the generation network. The first two columns show the authentic background and manipulation mask. As the number of epochs increases, the manipulated region matches better with the background and thus boundary artifacts are harder to identify.

segmentation network. Relying on boundary artifacts alone (**DL + G edge**) does not segment out entire manipulated regions, and yields poor hole filling. Additionally, directly predicting segmentation (**DL + G**) has a bias to semantic contents rather than manipulation artifacts, and thus has limited generalization ability. Furthermore, **GSR-Net** boosts the performance on **GS-Net** since the replacement stage introduces new boundary artifacts.

4.5. Robustness to Attacks

We apply both JPEG compression and scaling attacks to test images of Columbia and Carvalho datasets. We compare GSR-Net with RGB-N [38] and EXIF-selfconsistency [12] using their publicly available code, and MFCN [26] using the numbers reported in their paper. Figure 5 shows the results, which indicates our approach yields more stable performance than prior methods.

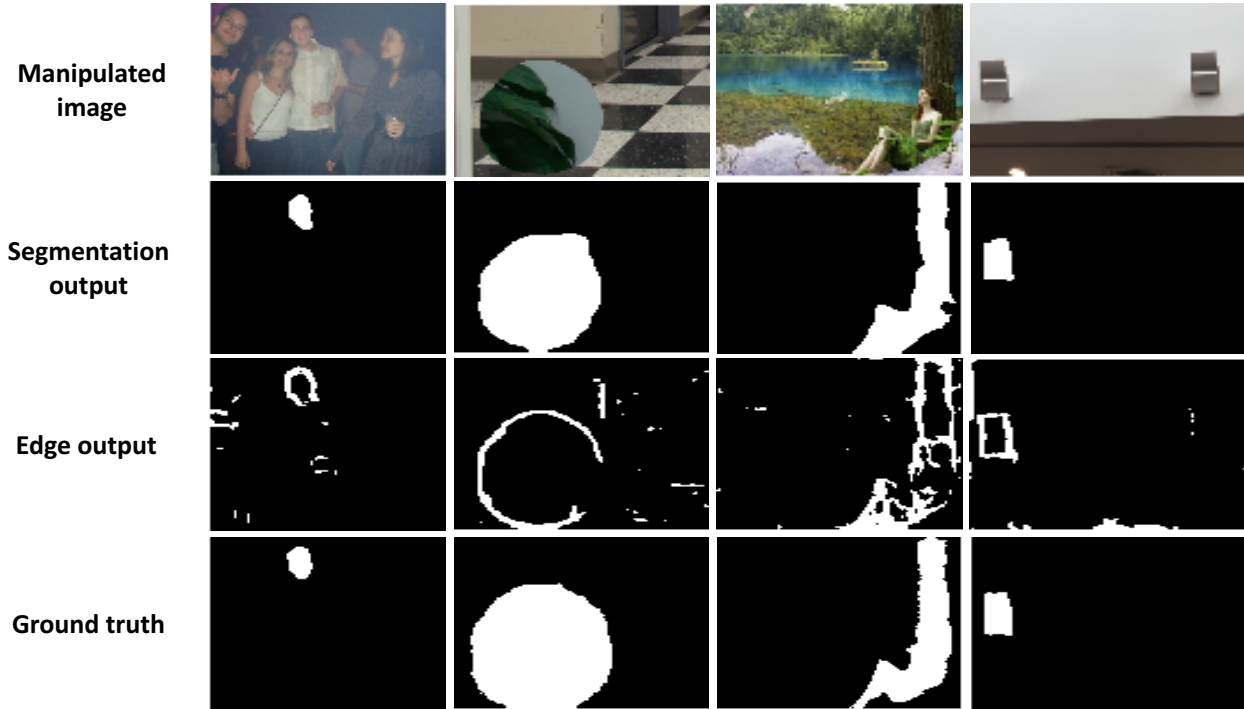


Figure 7. Qualitative visualization. The first row shows manipulated images on different datasets. The second indicates the final manipulation segmentation prediction. The third row illustrates the output of boundary artifacts branch. The last row is the ground truth.

4.6. Segmentation with COCO Annotations

This experiment shows how much gain our model achieves without using the manipulated images in CASIA 2.0. Without carefully manipulated training data, we only utilize the object annotations in COCO to create manipulated images. We compare the result of using different training data as follows:

- **cp + S**: Only using copy-pasted images to train the segmentation network.
- **cp_g + S**: Using both copy-pasted and generated images.
- **cp_g + SR**: Using copy-pasted images and generated images. The replacement stage is applied.

Table 3 presents the results. Surprisingly, the performance on Columbia only drops by a small margin. This might be because the splicing in Columbia is straightforward and copy-pasting provides enough information to segment the manipulated regions. The performance using only copy-pasted images (**cp + S**) on the four datasets indicates that our network truly learns boundary artifacts. Also, the improvement after adding generated images (**cp_g + S**) shows that our generation network provides useful manipulation examples that increases generalization. Last, the replacement stage (**cp_g + SR**) boosts performance further by encouraging the network to spot new boundary artifacts.

4.7. Qualitative Results

Generation Visualization. We illustrate some visualizations of the generation network in Figure 6. It is clear that the generation network learns to match the pasted region with background during training. As a result, the boundary artifacts are becoming subtle and the generation network produces hard examples for the segmentation network.

Segmentation Results. We present qualitative segmentation results on four datasets in Figure 7. Unsurprisingly, the boundary branch outputs the potential boundary artifacts in manipulated images and the other branch fills in the interior based on the predicted manipulated boundaries. The examples indicate that our approach deals well with both splicing and copy-move manipulation based on the manipulation clues from the boundaries.

5. Conclusion

We propose a novel manipulation segmentation network utilizing a generation network to increase generalization ability. Starting from easy examples, the generation network generates hard examples during training. We also design a boundary artifact guided segmentation network to focus on manipulation artifacts rather than semantic contents. Furthermore, we focus attention on artifacts through the replacement stage with no cost at inference time. Extensive experiments demonstrate the generalization ability of GSR-

Net on four standard datasets and show state-of-the-art performance. The manipulation segmentation problem is still far from being solved due to the large variation of manipulations and post-processing methods. Including more manipulation techniques in the generation network could potentially boost the generalization ability of the existing model and is part of our future research.

Acknowledgement

This work was supported by the DARPA MediFor program under cooperative agreement FA87501620191, “Physical and Semantic Integrity Measures for Media Forensics”.

References

- [1] M. Abadi, P. Barham, J. Chen, Z. Chen, A. Davis, J. Dean, M. Devin, S. Ghemawat, G. Irving, M. Isard, et al. Tensorflow: a system for large-scale machine learning. In *OSDI*, 2016. 5
- [2] J. H. Bappy, A. K. Roy-Chowdhury, J. Bunk, L. Nataraj, and B. Manjunath. Exploiting spatial structure for localizing manipulated image regions. In *ICCV*, 2017. 1, 2
- [3] L.-C. Chen, G. Papandreou, I. Kokkinos, K. Murphy, and A. L. Yuille. Deeplab: Semantic image segmentation with deep convolutional nets, atrous convolution, and fully connected crfs. In *TPAMI*, 2018. 4
- [4] Y. Cheng. Mean shift, mode seeking, and clustering. In *TPAMI*, 1995. 6
- [5] T. J. De Carvalho, C. Riess, E. Angelopoulou, H. Pedrini, and A. de Rezende Rocha. Exposing digital image forgeries by illumination color classification. In *TIFS*, 2013. 1, 5, 6
- [6] J. Deng, W. Dong, R. Socher, L.-J. Li, K. Li, and L. Fei-Fei. Imagenet: A large-scale hierarchical image database. In *CVPR*, 2009. 5
- [7] J. Dong, W. Wang, and T. Tan. Casia image tampering detection evaluation database 2010. <http://forensics.idealtest.org>. 1, 5, 6
- [8] J. Dong, W. Wang, and T. Tan. Casia image tampering detection evaluation database. In *ChinaSIP*, 2013. 1, 5
- [9] P. Ferrara, T. Bianchi, A. De Rosa, and A. Piva. Image forgery localization via fine-grained analysis of cfa artifacts. In *TIFS*, 2012. 6
- [10] I. Goodfellow, J. Pouget-Abadie, M. Mirza, B. Xu, D. Warde-Farley, S. Ozair, A. Courville, and Y. Bengio. Generative adversarial nets. In *NIPS*, 2014. 1
- [11] S. Hochreiter and J. Schmidhuber. Long short-term memory. *Neural computation*, 1997. 3
- [12] M. Huh, A. Liu, A. Owens, and A. A. Efros. Fighting fake news: Image splice detection via learned self-consistency. In *ECCV*, 2018. 1, 2, 5, 6, 7
- [13] S. Ioffe and C. Szegedy. Batch normalization: Accelerating deep network training by reducing internal covariate shift. In *ICML*, 2015. 5
- [14] P. Isola, J.-Y. Zhu, T. Zhou, and A. A. Efros. Image-to-image translation with conditional adversarial networks. In *CVPR*, 2017. 1, 3, 4, 5
- [15] D. P. Kingma and J. Ba. Adam: A method for stochastic optimization. In *ICLR*, 2015. 5
- [16] J.-F. Lalonde and A. A. Efros. Using color compatibility for assessing image realism. In *ICCV*, 2007. 3
- [17] H. Le, T. F. Y. Vicente, V. Nguyen, M. Hoai, and D. Samaras. A+ d net: Training a shadow detector with adversarial shadow attenuation. In *ECCV*, 2018. 3
- [18] T.-Y. Lin, M. Maire, S. Belongie, J. Hays, P. Perona, D. Ramanan, P. Dollár, and C. L. Zitnick. Microsoft coco: Common objects in context. In *ECCV*, 2014. 3
- [19] J. Long, E. Shelhamer, and T. Darrell. Fully convolutional networks for semantic segmentation. In *CVPR*, 2015. 2
- [20] B. Mahdian and S. Saic. Using noise inconsistencies for blind image forensics. In *IMAVIS*, 2009. 6
- [21] T.-T. Ng, J. Hsu, and S.-F. Chang. Columbia image splicing detection evaluation dataset. <http://www.ee.columbia.edu/ln/dvmm/downloads/AuthSplicedDataSet/AuthSplicedDataSet.htm/>, 2009. 1, 5, 6
- [22] J. Park, D. Cho, W. Ahn, and H.-K. Lee. Double jpeg detection in mixed jpeg quality factors using deep convolutional neural network. In *ECCV*, 2018. 1, 2
- [23] D. Pathak, P. Krahenbuhl, J. Donahue, T. Darrell, and A. A. Efros. Context encoders: Feature learning by inpainting. In *CVPR*, 2016. 3
- [24] P. Pérez, M. Gangnet, and A. Blake. Poisson image editing. In *TOG*, 2003. 3
- [25] O. Ronneberger, P. Fischer, and T. Brox. U-net: Convolutional networks for biomedical image segmentation. In *MICCAI*, 2015. 3
- [26] R. Salloum, Y. Ren, and C.-C. J. Kuo. Image splicing localization using a multi-task fully convolutional network (mfcn). In *JVCI*, 2018. 1, 2, 5, 6, 7
- [27] A. Shrivastava, T. Pfister, O. Tuzel, J. Susskind, W. Wang, and R. Webb. Learning from simulated and unsupervised images through adversarial training. In *CVPR*, 2017. 3
- [28] K. Simonyan and A. Zisserman. Very deep convolutional networks for large-scale image recognition. In *ICLR*, 2015. 4
- [29] N. Srivastava, G. Hinton, A. Krizhevsky, I. Sutskever, and R. Salakhutdinov. Dropout: a simple way to prevent neural networks from overfitting. In *JMLR*, 2014. 5
- [30] Y.-H. Tsai, X. Shen, Z. Lin, K. Sunkavalli, X. Lu, and M.-H. Yang. Deep image harmonization. In *CVPR*, 2017. 3
- [31] T.-C. Wang, M.-Y. Liu, J.-Y. Zhu, A. Tao, J. Kautz, and B. Catanzaro. High-resolution image synthesis and semantic manipulation with conditional gans. In *CVPR*, 2018. 3
- [32] X. Wang, A. Shrivastava, and A. Gupta. A-fast-rCNN: Hard positive generation via adversary for object detection. In *CVPR*, 2017. 3
- [33] Y. Wei, J. Feng, X. Liang, M.-M. Cheng, Y. Zhao, and S. Yan. Object region mining with adversarial erasing: A simple classification to semantic segmentation approach. In *CVPR*, 2017. 3, 5
- [34] B. Wen, Y. Zhu, R. Subramanian, T.-T. Ng, X. Shen, and S. Winkler. Coveragea novel database for copy-move forgery detection. In *ICIP*, 2016. 1, 5, 6

- [35] R. A. Yeh, C. Chen, T.-Y. Lim, A. G. Schwing, M. Hasegawa-Johnson, and M. N. Do. Semantic image inpainting with deep generative models. In *CVPR*, 2017. [1](#)
- [36] M. Zampoglou, S. Papadopoulos, and Y. Kompatsiaris. Large-scale evaluation of splicing localization algorithms for web images. In *MTAP*, 2017. [6](#)
- [37] P. Zhou, X. Han, V. I. Morariu, and L. S. Davis. Two-stream neural networks for tampered face detection. In *CVPRW*, 2017. [2](#)
- [38] P. Zhou, X. Han, V. I. Morariu, and L. S. Davis. Learning rich features for image manipulation detection. In *CVPR*, 2018. [1](#), [2](#), [5](#), [6](#), [7](#)